RSC Advances

ROYAL SOCIETY OF CHEMISTRY

www.rsc.org/advances

Electrocatalytic activity of Metalloporphyrins in situ grown on graphene sheets toward the oxygen reduction reaction in alkaline medium

Liqing Jiang,[a] Meng Li,[a] Lin Lin,[a] Yongfeng Li,[a] Xingquan He,[*a] Lili Cui[*a]

[a]*Department of Chemistry and Chemical Engineering, Changchun University of Science and Technology, Changchun 130022, P. R. China*

[*] Corresponding author. Tel.+86-431-85583430

E-mail address:hexingquan@hotmail.com (Xing-Quan He), cuilili1127@gmail.com (Li-Li Cui).

Abstract A series of non-noble-metal catalysts for the oxygen reduction reaction (ORR), based on metal 5,10,15,20-tetrakis(4-hydroxyphenyl)porphyrin (M-THPP, M: Fe^{3+}, Co^{2+}, Ni^{2+}, Mn^{2+}) grown on poly(sodium-p-styrenesulfonate) modified reduced graphene oxide (PSS-rGO), were fabricated using an in situ solvothermal synthesis method. The morphology of M-THPP/PSS-rGO was characterized by scanning electron microscopy (SEM) and transmission electron microscopy (TEM). Ultraviolet-visible (UV-vis) absorption spectroscopy and X-ray photoelectron spectroscopy (XPS) techniques were utilized to analyse the unusual interactions between metalloporphyrins and graphene sheets. Electrochemical measurements, such as rotating disk electrode (RDE) and rotating ring-disk electrode (RRDE) techniques, were employed to study the catalytic activity and the ORR mechanism of the oxygen reduction reaction on as-synthesised M-THPP/PSS-rGO catalysts in alkaline medium. The half-wave potential for the ORR on the CoTHPP/PSS-rGO catalyst was found to be around -0.22 V *vs*. SCE, which was much higher than those on other M-THPP/PSS-rGO catalysts, and similar to that on Pt/C (-0.20 V *vs*. SCE). RDE and RRDE results display that the ORR process proceeds mainly via almost 4-electron pathway on CoTHPP/PSS-rGO. The catalyst stability tests disclose that the CoTHPP/PSS-rGO is much stable than other M-THPP/PSS-rGO composites. The assembled CoTHPP/PSS-rGO catalyst possesses high activity, good long-term stability, excellent tolerance to the crossover effect of methanol and a facile 4-electron pathway for the ORR, which could be used as a promising Pt-free catalyst in alkaline direct methanol fuel cell.

Keywords: Metalloporphyrins; Graphene; Solvothermal synthesis; ORR

1. Introduction

With its high power density, high energy-conversion efficiency, scalability and low or zero emission of pollutants, direct methanol fuel cell (DMFC) has been paid much attention during the past few decades [1-3]. DMFC is made up of a Pt-Ru anode for methanol oxidation, a Pt cathode for oxygen reduction, and a proton exchange membrane (PEM) [1]. DMFC operates by oxidizing methanol to CO_2 and reducing oxygen to water [1,3,4]. Usually the electrochemical reduction of O_2 is a multi-electron reaction with a sluggish kinetics [5,6]. In alkaline media, the ORR mechanism can be expressed as reactions (1) and (2),

$$O_2 + H_2O + 2e^- \rightarrow HO_2^- + OH^- \quad (1)$$

$$O_2 + 2H_2O + 4e^- \rightarrow 4OH^- \quad (2)$$

To the best of our knowledge, the transfer of two electrons to produce H_2O_2 (HO_2^-) is potentially hazardous and less exoergic [6,7]. To achieve maximum energy-efficiency capacity, it is highly desirable to reduce O_2 via the direct four-electron pathway. In this respect, Pt-based materials or Pt is known to be the most efficient catalyst since it provides the highest current response toward the direct four-electron reduction of oxygen to water [6,8-12]. Due to not only the rarity and expensiveness but also the poor tolerance to the crossover effect and instability of Pt [6,13-15], however, numerous non-precious catalysts have been developed and screened in terms of their oxygen reduction reaction (ORR) for replacing Pt, including heteroatom (boron, nitrogen, sulfur, phosphorus) doped carbon nanomaterials [16-21], metal oxide/carbide/nitride materials [22-26], transition-metal chalcogenides [27,28],

N-containing polymers [29-32] and MN_4-centers of transition metal N_4-macrocycles [33-39]. Among them, transition metal N_4-macrocycles, especially transition metal porphyrins and phthalocyanines, due to their large π-conjugated aromatic systems with unique structures and coordination properties [40,41], thermal and chemical robustness [40], and rich electronic properties [42], have been received remarkable attention since Jasinski used cobalt phthalocyanine as an electrocatalyst for the ORR [43]. Therefore, a great number of transition metal N_4-macrocycles with different substitutes and central metals have been designed and applied to fabricate modified electrodes for the ORR [44-46]. However, as semiconductor materials [40], all these transition metal N_4-macrocycles still suffer from low activity and stability toward the ORR and thus are far from satisfying the requirements of commercialization of fuel cells.

Carbon nano-materials (CNMs), such as carbon powder, graphene, carbon nanotubes, due to themselves interesting physicochemical properties [47-49], such as excellent electrical conductivity, large specific surface area and high chemical stability, are more suitable for catalyst supports [40]. Recently, many researchers concentrate on CNMs-supported transition metal N_4-macrocycles materials. The purpose of using CNMs to support transition metal N_4-macrocycles is that strong π-π interactions between CNMs and transition metal N_4-macrocycles can make transition metal N_4-macrocycle moieties load on CNMs closely, thus stabilizing the systems, and the most important aspect is that the formation of micro/nano composites could provide more active sites and create synergistic effect, significantly improving

catalytic activity for the ORR [47,49]. Mamurua et al. [50] used octabutylsulphonylphthalocyanine complexes of iron (FeOBSPc) and cobalt (CoOBSPc) supported on multi-walled carbon nanotube (MWCNT) platforms for electrocatalytic reduction of oxygen, and found that the MWCNT-FeOBSPc composite exhibited the best ORR activity involving a direct 4-electron mechanism. Jahan et al. [51] investigated the electrocatalytic properties of graphene-metalloporphyrin composite, and the fabricated catalysts showed a facile 4-electron ORR pathway, much higher selectivity toward the ORR and significant tolerance to the crossover effect of methanol compared with Pt/C catalyst. Morozan and co-workers [52] investigated cobalt and iron phthalocyanines or porphyrins supported on different carbon nanotubes toward the oxygen reduction reaction. Mo et al. [53] synthesized a novel FeTSPc/SWCNTs composite by facilely modifying single-walled carbon nanotubes (SWCNTs) with iron tetrasulfophthalocyanine (FeTSPc), and the hybrid displayed an even better specificity, long-term stability, tolerance to methanol crossover effect and resistance toward the CO poisoning effect than commercial Pt/C catalyst.

To date, CNMs-supported transition metal N_4-macrocycle complexes as electrocatalytic materials are generally fabricated through the following methods. (1) π-π interactions [51,54]; (2) layer-by-layer (LBL) assembly [55]; (3) solid-phase synthesis [40]; (4) covalent modification [56]; (5) solvothermal synthesis [57,58]. Among these methods, solvothermal synthesis is considered as an effective and commercially viable method due to the advantages, including the feasibility of

controlling the morphology, the accessibility of cheap raw materials, low growth temperature and relatively economic processing. Our group [57,58] have prepared iron phthalocyanine/graphene and cobalt tetranitrophthalocyanine/graphene micro/nano composites for the ORR through solvothermal processes. These two catalysts all exhibited high catalytic activity, an almost 4-electron ORR pathway, much higher long-term stability and tolerance to methanol crossover effect comparable with Pt/C catalyst. In this study, a series of non-noble-metal catalysts for the ORR, including FeTHPP/PSS-rGO, CoTHPP/PSS-rGO, NiTHPP/PSS-rGO and MnTHPP/PSS-rGO, were fabricated by an in situ solvothermal synthesis method similar to our previous report [58]. The electrocatalytic performance and ORR mechanism on the M-THPP/PSS-rGO composites were discussed based on cyclic voltammetry, rotating disk electrode (RDE) and rotating ring-disk electrode (RRDE) measurements. Among fabricated electrocatalysts, it was found that the CoTHPP/PSS-rGO composite displayed high activity, good long-term stability, excellent tolerance to the crossover effect of methanol and an almost direct 4-electron pathway toward the ORR in alkaline solution, which could be viewed as a promising cathode candidate for alkaline direct methanol fuel cell application.

2. Experimental section

2.1 Chemicals

5,10,15,20-tetrakis(4-hydroxyphenyl)porphyrin (THPP) was synthesised as described in literature [59]. Pyrrole and p-hydroxy benzaldehyde were provided by Aladdin.

Natural graphite powder was purchased from Sigma-Aldrich. Reagents including H_2SO_4 (98 %), $NaNO_3$, $KMnO_4$, H_2O_2 (30 %), NaOH, metal chloride, DMF, propionic acid were analytical grade without further purification. Poly(sodium-p-styrenesulfonate) (PSS), hydrazine hydrate and Pt/C (20 wt % Pt on Vulcan XC-72) were bought from Alfa Aesar. Distilled water was used throughout the experiments.

2.2 Synthesis of graphite Oxide (GO) and poly(sodium-p-styrenesulfonate) modified reduced graphene oxide (PSS-rGO)

GO was synthesised from graphite powder by a modified Hummers' method [60,61]. PSS-rGO was obtained according to the literature procedures [62]. First, a GO aqueous colloidal suspension (200 mL, 1 mg mL^{-1}) was prepared by ultrasonically dispersing the paper-like graphite oxide in distilled water. Then, 2 g of poly(sodium-p-styrenesulfonate) was added with constantly stirring for 12 h at ambient temperature and pressure. Afterwards, 4 mL of hydrazine hydrate was slowly added to the mixture, which was heated to 95 °C and continuously stirred for 24 h. After cooling to room temperature, the mixture was separated by centrifugation and washed with distilled water for five times. Finally, the precipitate was dispersed into DMF by ultrasonic treatment, resulting in the PSS-rGO suspension (1.4 mg mL^{-1}).

2.3 Synthesis of M-THPP/PSS-rGO composites

The M-THPP/PSS-rGO composites were prepared by in situ solvothermal synthesis method. The synthesis routes of M-THPP/PSS-rGO are shown in Scheme 1. In a typical experiment, THPP (0.1031 mmol, 7 mg), metal chloride (0.3093 mmol) and

PSS-rGO (5 mL, 1.4 mg mL^{-1}) dispersion were added into 10 mL of DMF. The mixture was sonicated for 30 min. Subsequently, the stable suspension was sealed in a Telfon-lined autoclave and solvothermally treated at 150 °C for 6 h, then cooled to room temperature. The composite suspension was centrifuged, and the residue was washed with DMF, distilled water and alcohol in turn for three times.

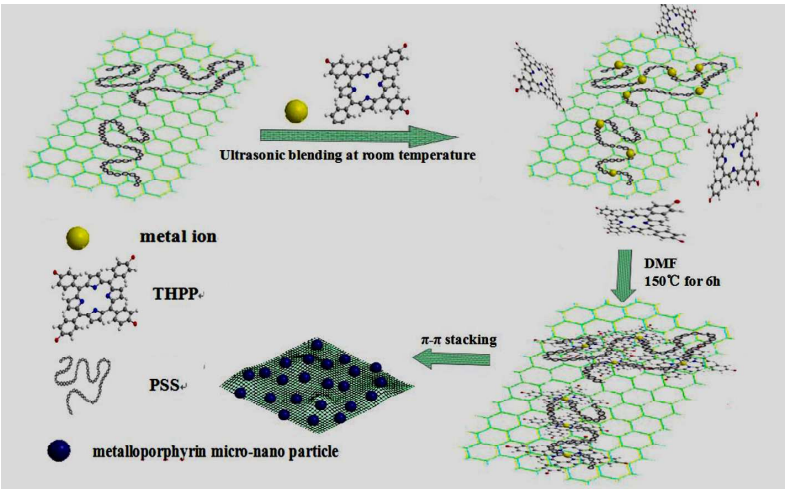

Scheme 1 The synthesis routes of M-THPP/PSS-rGO composites.

2.4 Characterization

For morphology characterization, scanning electron microscopy (SEM) and transmission electron microscopy (TEM) images were collected on JSM-6701F field emission scanning electron microscope operating at 5 kV and JEOL JEM-1200EX transmission electron microscope operating at 100 kV, respectively. UV-vis spectra were recorded using a mini UV-1240 spectrophotometer. The surface characterization of the synthesized samples was conducted by X-ray photoelectron spectroscopy (XPS, ESCLAB 250 spectrometer) using Al Kα X-ray source (1486.6 eV photons).

2.5 Electrode preparation and electrochemical measurements

A catalyst ink (1.0 mg mL^{-1}) was prepared by ultrasonically blending 10 mg of catalyst with 10 mL of alcohol. The ink was deposited onto a freshly polished glassy carbon (GC) electrode, and the coated electrode was then left to air dry. The total catalyst loading on the GC electrode was calculated to be 0.283 mg cm^{-2}. For comparison, the Pt/C or PSS-rGO modified GC electrode was also prepared as the same procedures above.

Electrochemical measurements, including cyclic voltammetry (CV), rotating disk electrode (RDE) and rotating ring-disk electrode (RRDE), were accomplished by a computer-controlled potentiostat (CHI660E electrochemical workstation, CH Instrument, USA) with a three-electrode cell system, in which the modified GC electrode with catalyst was employed as the working electrode, a platinum-wire electrode as the auxiliary electrode, a saturated calomel electrode (SCE) as the reference electrode. Cyclic voltammetry measurements were conducted at a GC electrode (CHI104, 3 mm in diameter) in N_2- or O_2-saturated 0.1 M NaOH electrolyte. The potential range was cyclically scanned between -0.8 V and +0.4 V *vs.* SCE at the scan rate of 100 mV s^{-1} at room temperature. RDE measurements were conducted at a GC rotating-disk electrode (5 mm in diameter) in O_2-saturated 0.1 M NaOH solution with the scan rate of 10 mV s^{-1}. Linear sweep voltammetry measurement (LSV) were scanned between -0.8 V and +0.2 V *vs.* SCE at different rotating speeds from 100 to 2500 rpm. Long-term chronoamperometric experiments were performed at the constant rotation speed of 1600 rpm. The RRDE data were obtained using a Pine Instrument Company AF-MSRCE modulator speed rotator. The working electrode

was a glassy carbon disk (5.61 mm in diameter) and a platinum ring (collection efficiency N = 0.37). An O_2-saturated 0.1 M NaOH aqueous solution was used as the electrolyte. The potential of the disk electrode was varied from -0.8 V to +0.2 V *vs*. SCE at the scan rate of 10 mV s^{-1}, and the ring potential was set at 0.1 V *vs*. SCE.

3. Results and discussion

3.1 Characterizations of M-THPP/PSS-rGO composites

Scanning electron microscopy (SEM) and transmission electron microscopy (TEM) were used for observing the surface morphology of the prepared samples. As is seen from Fig. 1A and C, the PSS-rGO displays a flexibly aggregated, crumpled nanosheet structure. For CoTHPP/PSS-rGO (Fig. 1B and D), we can observe nanoparticles closely stacked on the graphene sheet surface. The average diameter of nanoparticles is around 25 nm. Fig. 1E presents TEM image of CoTHPP nanoparticles alone fabricated via in situ solvothermal synthesis method, and the morphology and average diameter of CoTHPP nanoparticles is the same with nanoparticles coated on graphene, demonstrating that those nanoparticles on the graphene surface correspond to cobaltoporphyrin.

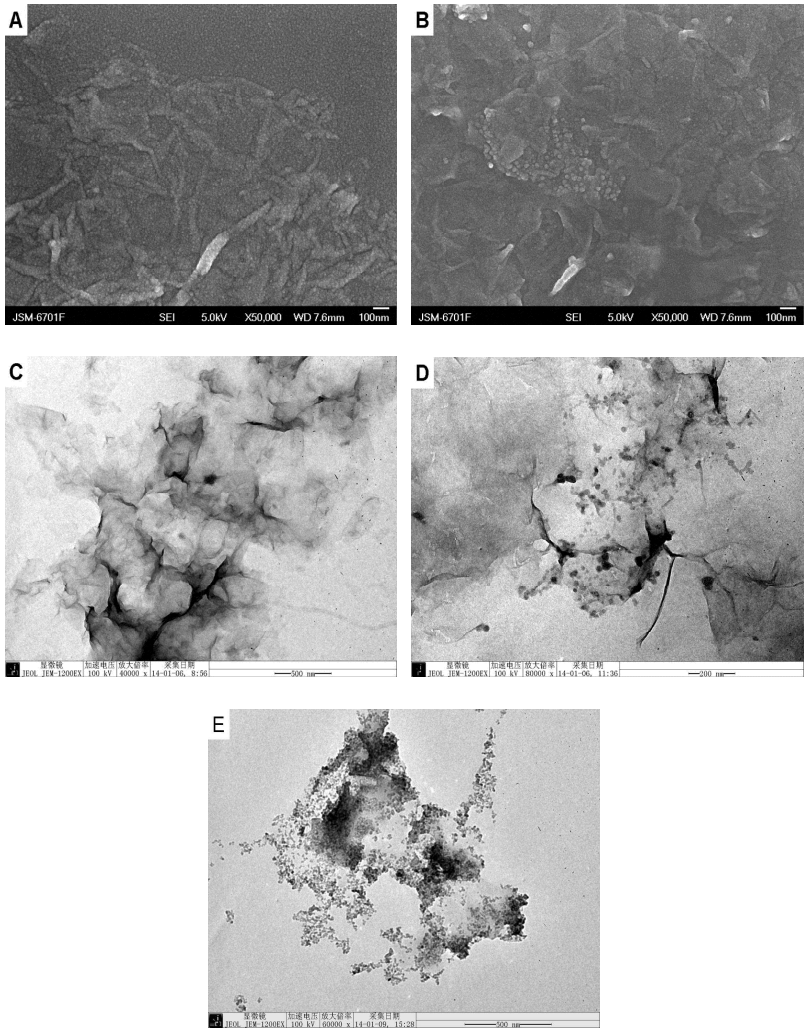

Fig. 1 SEM images of (A) PSS-rGO and (B) CoTHPP/PSS-rGO (1:1) are under higher ×50000 magnification; TEM images of (C) PSS-rGO ,(D) CoTHPP/PSS-rGO (1:1) and (E) CoTHPP are under higher magnification (×40000, ×80000 and ×60000 respectively).

The formation of the M-THPP/PSS-rGO hybrid should be related to the following facts. The negatively charged PSS modified on graphene can not only prevent the graphene sheets from stacking, but also adsorb the positively charged metal ions by electrostatic interaction. Meanwhile, the adsorbed metal ions react with metal-free porphyrin molecules under the solvothermal conditions, M-THPP is synthesized and

in situ coated on PSS-rGO. The M-THPP molecules that adsorbed on graphene can be served as "nuclei" for π-π assembly between M-THPP moieties and PSS-rGO sheets, leading to the formation of a randomly aggregated mico/nano hybrid.

The unusual interactions between metalloporphyrins and PSS-rGO sheets were monitored by UV-vis spectrometer and X-ray photoelectron spectrometer (XPS), respectively. Fig. 2a shows UV-vis spectra of PSS-rGO, CoTHPP and CoTHPP/PSS-rGO in alcohol solution. It can be seen that bare PSS-rGO shows a distinct absorption peak at 267 nm, the CoTHPP displays a strong Soret band peak at 432 nm, and two weaker Q band peaks at 543 nm and 584 nm, respectively. However, the CoTHPP/PSS-rGO composite exhibits a Soret band absorbance (436 nm) with a red-shift of 4 nm compared with CoTHPP. Furthermore, the Soret band absorbance of other M-THPP/PSS-rGO composites also displays different degrees of red-shift (Supplementary Fig. S1). These results indicate there were π-π interactions between M-THPP moieties and PSS-rGO sheets.

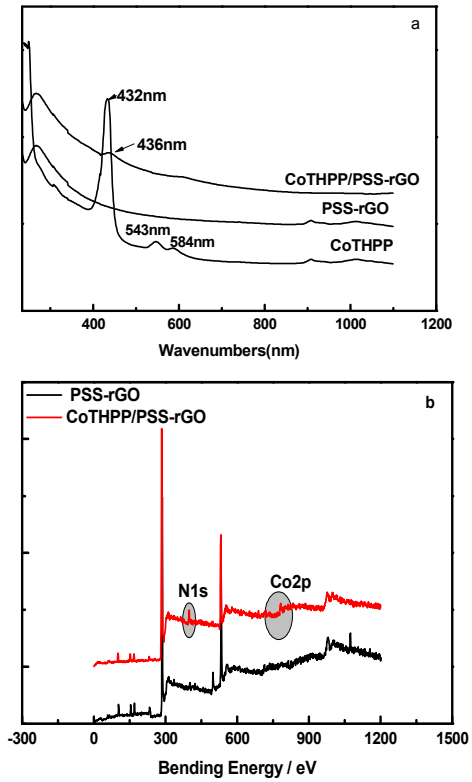

Fig. 2 (a) UV-vis absorption spectra of PSS-rGO, CoTHPP and CoTHPP/PSS-rGO, respectively; (b) XPS spectra of PSS-rGO and CoTHPP/PSS-rGO.

Except for UV-vis spectra, the interactions between metalloporphyrin moieties and PSS-rGO sheets were confirmed by XPS. By comparison of XPS survey spectra of PSS-rGO and M-THPP/PSS-rGO, we can confirm the presence of metalloporphyrins in M-THPP/PSS-rGO as the characteristic N1s peaks exist in all composites (shown in Fig. 2b and Supporting Information Fig. S2). In addition to the N1s signals, various metal 2p signals in Fig. 2b and Fig. S2 are also visible due to the metallic center of porphyrin. Fig. 3a, b shows the N1s high-resolution XPS spectra for CoTHPP/PSS-rGO and CoTHPP. From decomposition of the N1s XPS spectrum, the

spectrum for cobaltoporphyrin can be well fitted to two peaks with roughly equal area. The higher binding energy signal corresponds to pyrrolic-like nitrogen, the lower binding energy signal to pyridine-like nitrogen [63,64]. In contrast to CoTHPP, for CoTHPP/PSS-rGO, the N1s peaks of the pyrrolic- and pyridine-like nitrogen atoms shift to higher binding energies by 0.16 eV and 0.44 eV, respectively (Fig. 3a, b). From Fig. 3c, d, it can be seen that, compared with free CoTHPP, the binding energies of Co2p in CoTHPP/PSS-rGO shift from 781.29 eV ($2p_{3/2}$) and 796.38 eV ($2p_{1/2}$) [65] to 781.76 eV ($2p_{3/2}$) and 797.62 eV ($2p_{1/2}$), respectively. For other M-THPP/PSS-rGO composites, the same phenomenon as CoTHPP/PSS-rGO can also be observed (Supplementary Fig. S3). Such a pronounced shift of either N1s or metal 2p in binding energy further demonstrates that there exist strong electronic interactions between metalloporphyrin moieties and PSS-rGO sheets.

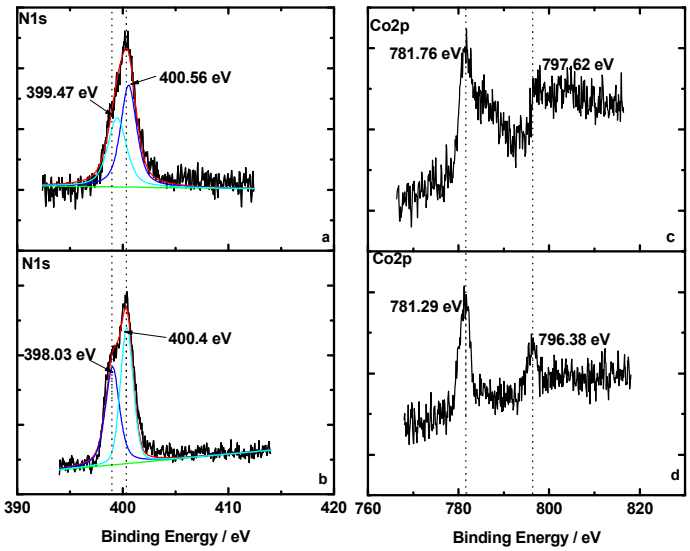

Fig. 3 High-resolution N1s and Co2p XPS spectra of (a), (c) CoTHPP/PSS-rGO and (b), (d) CoTHPP, respectively.

3.2 Electrochemical behavior of M-THPP/PSS-rGO in the oxygen reduction reaction

Fig. 4a shows the Cyclic voltammetry curves of CoTHPP/PSS-rGO and THPP/PSS-rGO modified electrodes in either N_2 or O_2 saturated 0.1 M NaOH solution. As shown in Fig. 4a, in the presence of N_2 saturated, no distinguished current response can be seen on THPP/PSS-rGO when the potential was cycled between −0.8 and 0.40 V *vs.* SCE. In contrast, the Cyclic voltammetry curve of CoTHPP/PSS-rGO presents a pair of nearly symmetrical redox peaks (0.1 V *vs.* SCE), which should be attributed to the redox transformation of CoN_4 center. In Fig. 4a, however, a well-defined oxygen reduction peak (-0.24 V *vs.* SCE) can be found on the CoTHPP/PSS-rGO composite when the Cyclic voltammetry was conducted in O_2-saturated 0.1 M NaOH solution, suggesting the high catalytic activity of the CoTHPP/PSS-rGO composite toward the ORR.

Supplementary Fig. S4 displays the cyclic voltammogram curves of CoTHPP/PSS-rGO with different mass ratio of THPP to PSS-rGO in O_2-staturated 0.1 M NaOH solution. In Fig. S4, when the initial ratio of THPP to PSS-rGO was 2:1, the peak potential (E_p) and peak current density of the ORR on CoTHPP/PSS-rGO can be observed to be around -0.34 V *vs*. SCE and 1.98 mA cm^{-2}, respectively. When the mass ratio of THPP to PSS-rGO varies from 2:1 to 1:1, the cathodic peak potential for oxygen reduction gradually shifts to more positive value from -0.34 V to -0.24 V *vs.* SCE, the peak current density also increases to 3.32 mA cm^{-2}. Whereas, when the mass ratio of THPP to PSS-rGO varies from 1:1 to 1:6, the peak current density

increases slowly, but the E_p shifts to more negative value. Therefore, the CoTHPP/PSS-rGO composite with 1:1 mass ratio of THPP to PSS-rGO was employed in the following study because of the most positive E_p and higher peak current density.

Fig. 4b depicts the Cyclic voltammetry curves of CoTHPP/PSS-rGO, PSS-rGO and CoTHPP modified GC electrodes in either N_2 or O_2 saturated 0.1 M NaOH solution, respectively. As is shown that, the ORR E_p of CoTHPP/PSS-rGO is 103 mV and 197 mV *vs.* SCE more positive than those of PSS-rGO and CoTHPP, respectively, and the current density on CoTHPP/PSS-rGO is more than twice as large as those on PSS-rGO and CoTHPP. The results strongly indicate that the catalytic activity of CoTHPP was greatly improved by using graphene as a support, suggesting the synergistic effect of CoTHPP and PSS-rGO toward the ORR.

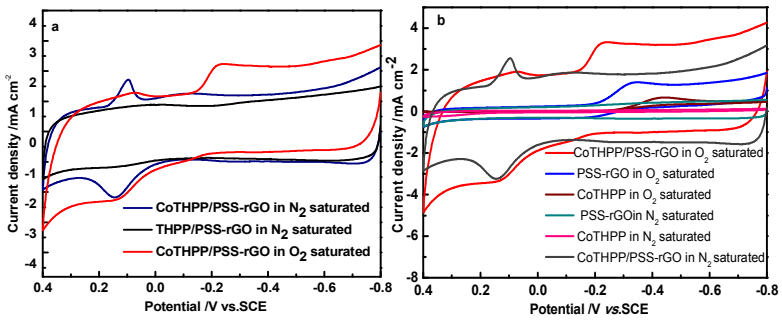

Fig. 4 Cyclic voltammetry curves of (a) CoTHPP/PSS-rGO and THPP/PSS-rGO in either N_2 or O_2 saturated 0.1 M NaOH solution. (b) CoTHPP/PSS-rGO, CoTHPP and PSS-rGO in either N_2 or O_2 saturated 0.1 M NaOH. Scan rate: 100 mV s^{-1}.

3.3 Mechanism of oxygen reduction on M-THPP/PSS-rGO composites

In order to verify the ORR mechanism quantitatively, our materials were loaded onto

GC electrodes for rotating-disk electrode (RDE) measurements. Fig. 5a shows RDE curves for CoTHPP/PSS-rGO at various rotation speeds (from 100 to 2500 rpm). The limiting current depicts a typical increase with rotation speeds owing to shortened diffusion layer [16]. Similar studies for other catalysts, including FeTHPP/PSS-rGO, MnTHPP/PSS-rGO, NiTHPP/PSS-rGO and PSS-rGO, are given in the supplementary section (Fig. S5 a1, a2, a3, a4). Fig. 5b shows a series of RDE curves of different catalysts including a commercial Pt/C (20 wt %) measured in O_2-saturated 0.1 M NaOH at the scan rate of 10 mV s^{-1} and rotation speed of 1600 rpm. To compare the activity of different catalysts with each other, the half-wave potential of each catalyst was estimated by determining the maxima of the derivatives of the reduction current (see table 1 for details). Notably, the CoTHPP/PSS-rGO is the most active catalyst among fabricated catalysts due to the high half-wave potential (-0.22 V *vs.* SCE), followed by MnTHPP/PSS-rGO (-0.32 V *vs.* SCE), FeTHPP/PSS-rGO (-0.38 V *vs.* SCE) and NiTHPP/PSS-rGO (-0.40 V *vs.* SCE), but not outperform commercial Pt/C catalyst (-0.20 V *vs.* SCE). The electrocatalytic activity of these hybrids appears thus to be greatly affected by the nature of the central metal. In addition, we also compare our catalyst with some recently reported similar hybrid materials using graphene and MN_4 complexes that have admirable performance for the cathodic ORR (seen in Supporting Information Table S1). In general, the performance of our CoTHPP/PSS-rGO catalyst is comparable with, or even better than those of the previous reports in terms of the onset potential, half-wave potential and limiting current density.

To shed light on the electrochemical kinetics of catalysts in the ORR, Tafel analysis was performed on these samples. Fig. S6 presents the Tafel curves which were derived from the polarization curves of Fig. 5b with the rotation rate of 1600 rpm. It can be seen that different catalysts will lead to different Tafel slope values. The Tafel slopes on various samples were listed in Table 1. Obviously, the Tafel slope on CoTHPP/PSS-rGO catalyst gives the smallest value in the low or high overpotential region. Generally, in the low overpotential region, the first electron transfer is the rate-determining step, and the oxygen reduction process is controlled by the kinetics of the surface reaction [67]. In the high overpotential region, the reaction rate is dominated by the diffusion limitation inside the material, which is commonly interpreted in terms of a two-electron transfer reaction as the rate-determining step [57].

On the basis of RDE voltammograms, we can calculate the number of electrons transferred (n) according to the Koutecky-Levich equation [33,37,51,68]:

$$\frac{1}{J} = \frac{1}{J_{\mathrm{L}}} + \frac{1}{J_{\mathrm{K}}} = \frac{1}{\mathrm{B}\omega^{1/2}} + \frac{1}{J_{\mathrm{K}}} \quad (1)$$

$$\mathrm{B} = 0.62nFC_0D_0^{2/3}\upsilon^{-1/6} \quad (2)$$

where J is the measured current density (mA cm^{-2}), J_{K} and J_{L} are the kinetic and diffusion-limited current densities, respectively, n is the electron transfer number for the reaction. F is the Faraday constant (96,500 C mol^{-1}). D_0 is the diffusion coefficient for oxygen in solution (2.0×10^{-5} cm^2 s^{-1}), υ is the kinematic viscosity of the electrolyte solution (0.001 cm^2 s^{-1}), C_0 is the concentration of O_2 in the air-saturated solution (0.25 mM), and ω is the rotation speed (rpm s^{-1}). All the parameters are invariant over

the potential range with the exception of n value. By plotting the graph between J^{-1} and $\omega^{-1/2}$, n value can be determined based on the slope of Koutecky-Levich plots.

Fig. 5c displays the Koutecky-Levich plots of CoTHPP/PSS-rGO for the ORR at fixed potentials of -0.4 V, -0.5 V, -0.6 V and -0.7 V *vs.* SCE, respectively, which were derived from RDE curves of CoTHPP/PSS-rGO obtained at various rotation speeds. Similar Koutecky-Levich plots for other catalysts are given in Supplementary Fig. S5 b1, b2, b3, b4. According to the Koutecky-Levich equation, the calculated n values for the ORR on M-THPP/PSS-rGO are shown in Fig. 5d. As Fig. 5d shown, however, the average electron transfer number n on most of M-THPP/PSS-rGO composites presents even bigger number than 4 over all the potential range. The reason, according to previous study [53,66], might be that the oxygen reduction pathways occurring on our materials were very complicated, involving not only the ORR but also the redox process of porphyrin ring. This means that the Koutecky-Levich equation was not reliable to accurately evaluate the electron transfer number per O_2 molecule.

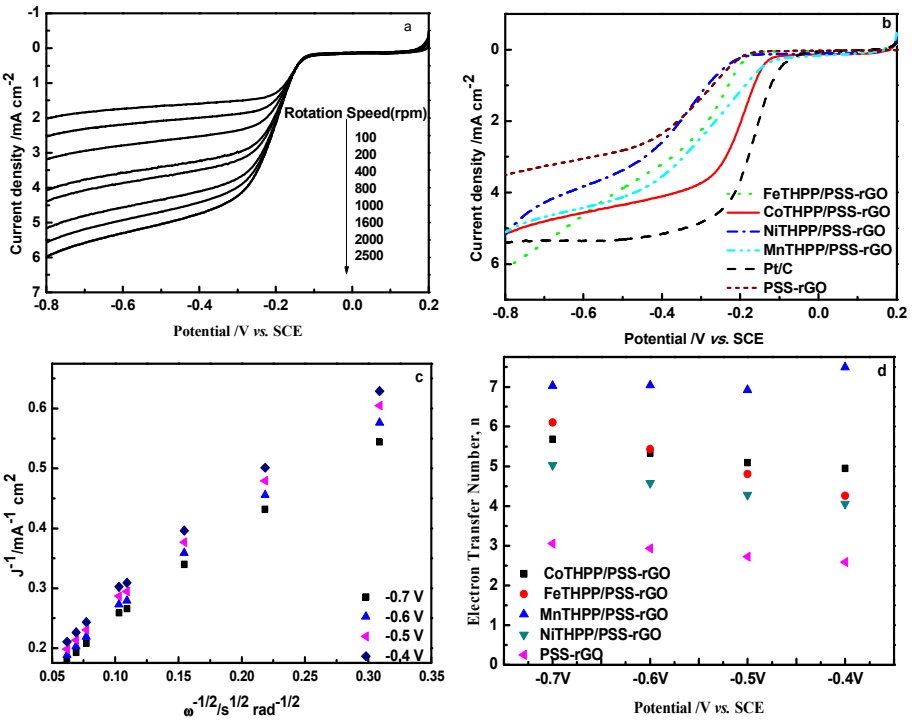

Fig. 5 (a) Linear sweep voltammograms of CoTHPP/PSS-rGO at different rotating speeds; (b) Linear sweep voltammograms of PSS-rGO, M-THPP/PSS-rGO and Pt/C at the rotation speed of 1600 rpm. (c) Koutecky-Levich plots of CoTHPP/PSS-rGO and (d) electron transfer number of PSS-rGO and M-THPP/PSS-rGO at fixed potentials of -0.4 V, -0.5 V, -0.6 V and -0.7 V *vs.* SCE, respectively.

Table 1. Electrocemical parameters for oxygen reduction estimated from polarization curves at 1600 rpm.

			Tafel plot slopes (mV dec^{-1})	
catlyst	$E_{1/2}$ /V *vs.* SCE	J_L/mA cm^{-2}	low η	high η
PSS-rGO	-0.34	3.51	139	538
NiTHPP/PSS-rGO	-0.40	5.16	117	484
MnTHPP/PSS-rGO	-0.32	5.11	113	449
FeTHPP/PSS-rGO	-0.38	6.15	83	454
CoTHPP/PSS-rGO	-0.22	5.16	61	366
Pt/C	-0.20	5.33	61	227

To accurately confirm the ORR mechanism of M-THPP/PSS-rGO composites,

rotating ring disk electrode (RRDE) technique was employed. The electron number (n) and the hydrogen peroxide ion yield (% HO_2^-) during the ORR can be determined by the following equations [46,54,69] :

$$\% \, HO_2^- = 200 \times \frac{I_r/N}{I_d + I_r/N} \quad (3)$$

$$n = 4 \times \frac{I_d}{I_d + I_r/N} \quad (4)$$

where N = 0.37 is the collection efficiency, I_d is the disk current, and I_r is the ring current.

Fig. 6a shows the I_d and I_r for FeTHPP/PSS-rGO, CoTHPP/PSS-rGO, NiTHPP/PSS-rGO and MnTHPP/PSS-rGO, respectively. The corresponding I_r for the oxidation of hydrogen peroxide ion (HO_2^-) was measured with a Pt ring electrode at the polarized potential of 0.10 V *vs.* SCE. On the basis of I_d and I_r, the electron transfer number (n) was calculated to be 3.69-3.80 for FeTHPP/PSS-rGO, 3.79-3.83 for CoTHPP/PSS-rGO, 3.19-3.72 for MnTHPP/PSS-rGO and 2.65-2.82 for NTHPP/PSS-rGO over the potential range from -0.8 V to +0.20 V *vs.* SCE (Fig. 6b). Fig. 6c displays the percentage of hydrogen peroxide ion yielded on the MTHPP/PSS-rGO composites in the same potential range. The trends in Fig. 6b and c indicate the ORR mechanism is strongly potential-dependent. Notably, the CoTHPP/PSS-rGO composite with n = 3.79-3.83 and % HO_2^- = 8.60-10.70 %, exhibits much higher activity over the whole potential range, emphasizing that the ORR process on CoTHPP/PSS-rGO proceeds mainly via a direct four-electron pathway.

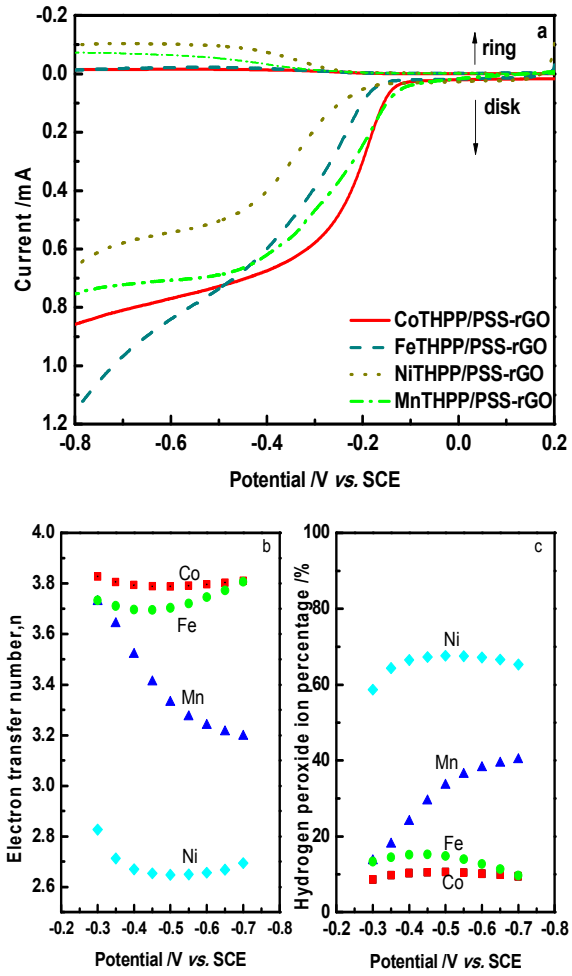

Fig. 6 (a) RRDE tests of the ORR on M-THPP/PSS-rGO in O_2-saturated 0.1 M NaOH at a rotation speed of 1600 rpm. The ring electrode is polarized at 0.1V *vs.* SCE. Scan rate: 10 mV s^{-1}. (b) Electron transfer number and (c) Hydrogen peroxide ion percentage of CoTHPP/PSS-rGO, FeTHPP/PSS-rGO, MnTHPP/PSS-rGO and NiTHPP/PSS-rGO as a function of electrode potential.

3.4 Study of stability and the methanol crossover effect

The long-term stability of catalysts is one of the major concerns in current DMFC technology. The stability of M-THPP/PSS-rGO and Pt/C was assessed through chronoamperometric measurements for 12 h in an O_2-saturated 0.1 M NaOH aqueous

solution at the rotation rate of 1600 rpm. As revealed in Fig. 7, the chronoamperometric response for CoTHPP/PSS-rGO exhibits a very slow attenuation with the highest current retention (75 %). In contrast, the corresponding current loss for Pt/C catalyst shows a fast decrease with the lowest retention (46 %) under the same conditions. Fig. 8 shows the Cyclic voltammetry curves of CoTHPP/PSS-rGO (a) and Pt/C (b) in O_2-saturated 0.1 M NaOH aqueous solution, in the presence/absence of 3 M methanol. In the absence of methanol, the obvious ORR peaks at -0.24 V and -0.21 V *vs.* SCE can be observed for CoTHPP/PSS-rGO and Pt/C. After adding 3 M methanol, for Pt/C, the ORR peak current obviously decreases and a new oxidation peak at 0.0 V *vs.* SCE appears (Fig. 8b), while there is no notable change in both peak potential and peak current for CoTHPP/PSS-rGO (Fig. 8a). We thus believe that our CoTHPP/PSS-rGO catalyst possesses excellent stability and can eliminate the negative effects of the methanol crossover.

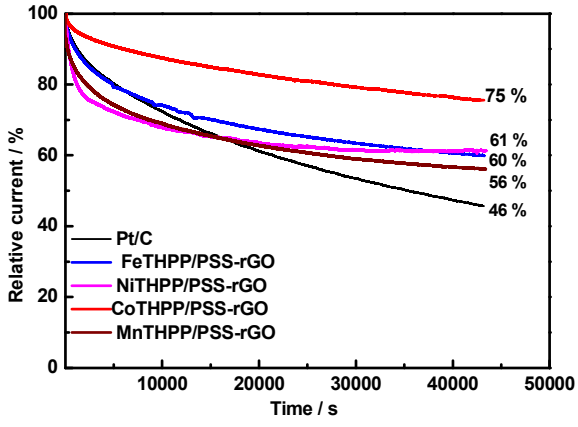

Fig. 7 The chronoamperometry curves of Pt/C and M-THPP/PSS-rGO in O_2-saturated 0.1 M NaOH with the rotation speed of 1600 rpm.

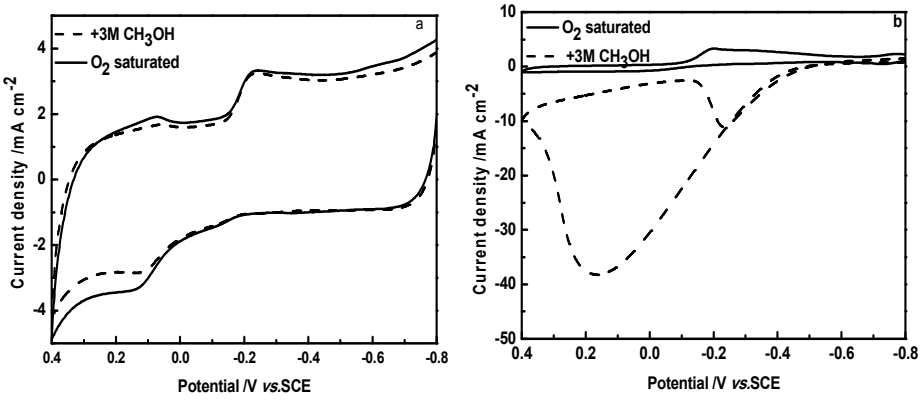

Fig. 8 Cyclic voltammetry curves of CoTHPP/PSS-rGO (a) and Pt/C (b) at the scan rate of 100 mV s^{-1} in O_2-saturated 0.1 M NaOH solution with and without 3 M CH_3OH.

4. Conclusions

In summary, we fabricated novel M-THPP/PSS-rGO composites via in situ solvothermal synthesis method. The SEM and TEM results demonstrated CoTHPP moieties were tightly anchored on the PSS-rGO surface. UV-vis and XPS spectra results suggested there were strong π-π interactions between M-THPP moieties and PSS-rGO sheets. Electrochemical measurements results disclosed that, among fabricated electrocatalysts, CoTHPP/PSS-rGO possessed high electrocatalytic activity, the best long-term stability, excellent tolerance to the crossover effect of methanol, especially, the more efficient 4-electron pathway toward the ORR in alkaline solution, which could be anticipated for the mass-production as the cathode catalyst candidate for alkaline direct methanol fuel cell.

Acknowledgements

The work has been supported by the Natural Science Foundation of China (No. 21273024) and Natural Science Foundation of Jilin Province, China (No. 201215135).

Reference

[1] S. Sundarrajan, S. I. Allakhverdiev and S. Ramakrishna, *Int. J. Hydrogen Energy*, 2012, **37**, 8765-8786.

[2] X. Zhao, M. Yin, L. Ma, L. Liang, C. P. Liu, J. H. Liao, T. H. Lu and W. Xing, *Energy Environ. Sci*., 2011, **4**, 2736-2753.

[3] Y. H. Lee, G. Lee, J. H. Shim, S. Hwang, J. Kwak, K. Lee, H. Song and J. T. Park, *Chem. Mater.*, 2006, **18**, 4209-4211.

[4] Y. F. Zhang, Z. Y. Yuan, S. B. Wang, H. He, Y. R. Zhao and X. W. Liu, *Energy Fuels*, 2010, **24**, 6449-6455.

[5] Z. Q. Jiang, Z. J. Jiang, X. N. Tian and W. H. Chen, *J. Mater. Chem. A*, 2014, **2**, 441-450.

[6] H. J. Yin, H. J. Tang, D. Wang, Y. Gao and Z. Y. Tang, *ACS Nano*, 2012, **6**, 8288-8297.

[7] A. Trojánek, J. Langmaier, S. Záliš and Z. Samec, *Electrochim. Acta*, 2013, **110**, 816-821.

[8] K. Sasaki, H. Naohara, Y. M. Choi, Y. Cai, W. F. Chen, P. Liu and R. R Adzic, *Nat. Commun.*, 2012, **3**, 1115-1124.

[9] D. L. Wang, Y. C. Yu, H. L. Xin, R. Hovden, P. Ercius, J. A. Mundy, H. Chen, J. H. Richard, D. A. Muller, F. J. DiSalvo and H. D. Abruña, *Nano Lett.*, 2012, **12**, 5230-5238.

[10] N. R. Elezović, B. M. Babić, Lj. Gajić-Krstajić, P. Ercius, V. R. Radmilović, N. V. Krstajić and Lj. M. Vračar, *Electrochim. Acta*, 2012, **69**, 239-246.

[11] Z. W. Chen, M. Waje, W. Z. Li and Y. S. Yan, *Angew. Chem. Int. Ed.*, 2007, **46**, 4060-4063.

[12] R. Lin, H. Y. Zhang, T. T. Zhao, C. H. Cao, D. J. Yang and J. X. Ma, *Electrochim. Acta*, 2012, **62**, 263-268.

[13] C. W. B. Bezerra, L. Zhang, K. C. Lee, H. S. Liu, A. L. B. Marques, E. P. Marques, H. J. Wang and J. J. Zhang, *Electrochim. Acta*, 2008, **53**, 4937-4951.

[14] C. X. Zhang, K. Yanagisawa, H. J. Tao, A. Onda, T. Shou and S. Kamiya, *Catal. Lett.*, 2012, **142**, 1128-1133.

[15] Y. W. Ma, H. M. Zhang, H. X. Zhong, T. Xu, H. Jin, Y. F. Tang and Z. Xu, *Electrochim. Acta*, 2010, **55**, 7945-7950.

[16] W. Yang, T. P. Fellinger and M. Antonietti, *J. Am. Chem. Soc.*, 2011, **133**, 206-209.

[17] D. H. Deng, X. L. Pan, L. Yu, Y. Cui, Y. P. Jiang, J. Qi, W. X. Li, Q. Fu, X. C. Ma, Q. K. Xue, G. Q. Sun and X. H. Bao, *Chem. Mater.*, 2011, **23**, 1188-1193.

[18] D. S. Yang, D. Bhattacharjya, S. Inamdar, J. Park and J. S. Yu, *J. Am. Chem. Soc.*, 2012, **134**, 16127-16130.

[19] R. Silva, D. A. Voiry, M. Chhowalla and T. Asefa, *J. Am. Chem. Soc*., 2013, **25**, 7823-7826.

[20] W. Y. Wonga, W. R. W. Daud, A. B. Mohamad, A. A. H. Kadhum, K. S. Loh and E. H. Majlan, *Int. J. Hydrogen Energy*, 2013, **38**, 9370-9386.

[21] S. B. Yang, L. J. Zhi, K. Tang, X. L. Feng, J. Maier and K. Müllen, *Adv. Funct. Mater*., 2012, **22**, 3634-3640.

[22] Y. Y. Liang, Y. G. Li, H. L. Wang, J. G. Zhou, J. Wang, T. Regier and H. J. Dai, *Nat. Mater.*, 2011, **10**, 780-786.

[23] Z. S. Wu, S. B. Yang, Y. Sun, K. Parvez, X. L. Feng and K. Müllen, *J. Am. Chem. Soc.*, 2012, **134**, 9082-9085.

[24] I. Roche, E. Chaînet, M. Chatenet and J. Vondrák, *J. Phys. Chem. C*, 2007, **111**, 1434-1443.

[25] Y. Ohgi, A. Ishihara, K. Matsuzawa, S. Mitsushima, K. I. Ota, M. Matsumoto and H. Ima, *Electrochim. Acta*, 2012, **68**, 192-197.

[26] J. H. Kim, A. Ishihara, S. Mitsushima, N. Kamiya and K. I. Ota, *Electrochim. Acta*, 2007, **52**, 2492-2497.

[27] Y. J. Feng and N. Alonso-Vante, *Phys. Status Solidi (b)*, 2008, **245**, 1792-1806.

[28] M. R. Gao, Y. F. Xu, J. Jiang and S. H. Yu, *Chem. Soc. Rev.*, 2013, **42**, 2986-3017.

[29] S. W. Yuan, J. L. Shui, L. Grabstanowicz, C. Chen, S. Commet, B. Reprogle, T. Xu, L. P. Yu and D. J. Liu, *Angew. Chem.*, 2013, **125**, 8507-8511.

[30] S. H. Lim, Z. T. Li, C. K. Poh, L. F. Lai and J. Y. Lin, *J. Power Sources*, 2012, **214**, 15-21.

[31] J. Wu, W. M. Li, D. Higgins and Z. W. Chen, *J. Phys. Chem. C*, 2011, **115**, 18856-18862.

[32] Q. Zhou, C. M. Li, J. Li and J. T. Lu, *J. Phys. Chem. C*, 2008, **112**, 18578-18583.

[33] U. B. Nasini, Y. Gartia, P. Ramidi, A. Kazi, A. U. Shaikh and A. Ghosh, *Chem. Phys. Lett.*, 2013, **566**, 38-43.

[34] W. M. Li, A. P. Yu, D. C. Higgins, B. G. Llanos and Z. W. Chen, *J. Am. Chem. Soc.*, 2010, **132**, 17056-17058.

[35] M. Isaacs, M. J. Aguirre, A. Toro-Labbé, J. Costamagna, M. Páez and J. H. Zagal, *Electrochim. Acta*, 1998, **43**, 1821-1827.

[36] B. Wang, *J. Power Sources*, 2005, **152**, 1-15.

[37] I. Kruusenberg, J. Mondal, L. Matisen, V. Sammelselg and K. Tammeveski, *Electrochem. Commun.*, 2013, **33**, 18-22.

[38] S. R. Sun, N. Jiang and D. G. Xia, *J. Phys. Chem. C*, 2011, **115**, 9511-9517.

[39] R. L. Liu, C. V. Malotki, L. Arnold, N. Koshino, H. Higashimura, M. Baumgarten and K. Müllen, *J. Am. Chem. Soc.*, 2011, **133**, 10372-10375.

[40] H. J. Li, Z. W. Xu, K. Z. Li, X. H. Hou, G. X. Cao, Q. L. Zhang and Z. Y. Cao, *J. Mater. Chem.*, 2011, **21**, 1181-1186.

[41] X. Feng, L. Chen, Y. P. Dong and D. L. Jiang, *Chem. Commun.*, 2011, **47**, 1979-1981.

[42] H. He, Y. K. Lei, C. Xiao, D. Y. Chu, R. R. Chen and G. F. Wang, *J. Phys. Chem. C*, 2012, **116**, 16038-16046.

[43] R. Jasinski, *Nature*, 1964, **201**, 1212-1213.

[44] W. Chen, J. Akhigbe, C. Brückner, C. M. Li, Y. Lei, *J. Phys. Chem. C*, 2010, **114**, 8633-8638.

[45] S. Swavey and A. Eder, *Inorg. Chem. Commun.*, 2013, **29**, 14-17.

[46] J. Masa and W. Schuhmann, *Chem.-Eur. J.*, 2013, **19**, 9644-9654.

[47] N. C. Cheng, C. Kemna, S. Goubert-Renaudin and A. Wieckowski, *Electrocatalysis*, 2012, **3**, 238-251.

[48] W. Zhang, A. U. Shaikh, E. Y. Tsui and T. M. Swager, *Chem. Mater.*, 2009, **21**, 3234-3241.

[49] G. L. Turdean, I. C. Popescu, A. Curulli and G. Palleschi, *Electrochim. Acta*, 2006, **51**, 6435-6441.

[50] S. A. Mamuru, K. I. Ozoemena, T. Fukuda, N. Kobayashi and T. Nyokong, *Electrochim. Acta*, 2010, **55**, 6367-6375.

[51] M. Jahan, Q. L. Bao and K. P. Loh, *J. Am. Chem. Soc.*, 2012, **134**, 6707-6713.

[52] A. Morozan, S. Campidelli, A. Filoramo, B. Jousselme and S. Palacin, *Carbon*, 2011, **49**, 4839-4847.

[53] G. Q. Mo, S. Y. Liao, Y. Z. Zhang, W. D. Zhang and J. S. Ye, *Electrochim. Acta*, 2012, **76**, 430-439.

[54] Y. Y. Jiang, Y. Z. Lu, X. Y. Lv, D. X. Han, Q. X. Zhang, L. Niu and W. Chen, *ACS Catal.*, 2013, **3**, 1263-1271.

[55] H. J. Tang, H. J. Yin, J. Y. Wang, N. L. Yang, D. Wang and Z. Y. Tang, *Angew. Chem. Int. Ed.*, 2013, **52**, 1-6.

[56] S. K. Kim and S. Jeon, *Electrochem. Commun.*, 2012, **22**, 141-144.

[57] L. L. Cui, G. J. Lv, Z. Y. Dou and X. Q. He, *Electrochim. Acta*, 2013, **106**, 272-278.

[58] G. J. Lv, L. L. Cui, Y. Y. Wu, Y. Liu, T. Pu and X. Q. He, *Phys. Chem. Chem. Phys.*, 2013, **15**, 13093-13100.

[59] A. C. Serra, M. Pineiro, A. M. d'A. Rocha Gonsalves, M. Abrantes, M. Laranjo, A. C. Santos and M. F. Botelho, *J. Photochem. Photobio. B*, 2008, **92**, 61-67.

[60] Y. X. Xu, L. Zhao, H. Bai, W. J. Hong, C. Li and G. Q. Shi, *J. Am. Chem. Soc.*, 2009, **131**, 13490-13497.

[61] J. X. Geng and H. T. Jung, *J. Phys. Chem. C* , 2010, **114**, 8227-8234.

[62] D. Q. Wu, F. Zhang, H. W. Liang and X. L. Feng, *Chem. Soc. Rev*., 2012, **41**, 6160-6177.

[63] A. Gulino, *Anal. Bioanal. Chem.,* 2013,**405**, 1479–1495.

[64] D. M. Sarno, L. J. Matienzo, and W. E. Jones, *J. Inorg. Chem.*, 2001, **40,** 6308-6315.

[65] K. Artyushkova, S. Levendosky, P. Atanassov, J. Fulghum, *Top Catal.*, 2007, **46**, 263–275.

[66] Y. Yuan, J. Ahmed and S. Kim, *J. Power Sources*, 2011, **196**, 1103-1106.

[67] M. T. de Groot, M. Merkx, A. H. Wonders and M. T. M. Koper, *J. Am. Chem. Soc.*, 2005, **127**, 7579-7586.

[68] R. R. Chen, H. X. Li, D. Y. Chu and G. F. Wang, *J. Phys. Chem. C*, 2009, **113**, 20689-20697.

[69] T. S. Olson, S. Pylypenko, J. E. Fulghum and P. Atanassov, *J. Electrochem. Soc.*, 2010, **157**, B54-B63.

Graphical Abstract

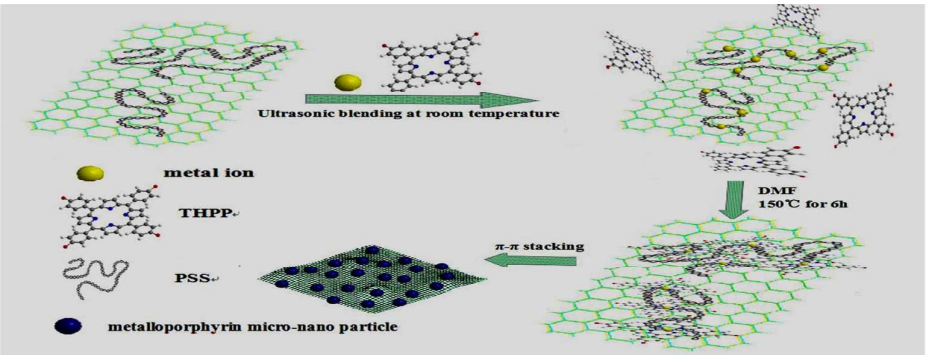

A series of novel non-noble-metal catalysts for ORR, based on metalloporphyrins grown on poly(sodium-p-styrenesulfonate) modified reduced graphene oxide sheets, have been successfully fabricated using an in situ solvothermal synthesis method.